AIAA-2003-3599

STUDIES OF TURBULENT MIXING USING THE VORCAT* IMPLEMENTATION OF THE 3D VORTEX METHOD

Peter S Bernard †
University of Maryland
College Park, MD

Mark Potts ‡
VorCat Inc.
Rockville, MD

Jacob Krispin §
VorCat Inc.
Rockville, MD

Abstract

By their grid-free character, vortex methods represent a natural complement to Lagrangian particle methods for the solution of two-phase particulate flows. With modern fast schemes for evaluating velocities from large collections of vortex elements, it becomes practical to treat three-dimensional turbulent, two-phase flows through grid-free technology. This paper describes an application of the VorCat implementation of the vortex method to the study of particulate dispersion in a spatially developing mixing layer. Some details of the computed vortex structure are described including the development of streamwise counter-rotating vortices in the braid regions, their effect upon spanwise rollers and the breakdown of the flow into turbulence. Particle dispersion in the mixing layer flow is examined including the effects of streamwise vorticity and two-way coupling between phases.

Introduction

Lagrangian schemes for simulating high Reynolds number two-phase particulate flows [5, 21] can provide a relatively natural representation of scalar mixing (e.g., free of the distortions associated with grid-based numerical diffusion) so long as the underlying computation of the turbulent flow field captures the rotational motions most associated with turbulent mixing. Grid-free vortex methods [18], in which the dynamics of the flow are represented through freely convecting and interacting vortical elements, are particularly well poised to supply information about the vortical eddies of turbulence including internal shear layers and other sharp interfaces that would otherwise be smoothed in grid-based methods. Consequently, there is considerable incentive for developing predictive methods combining grid-free vortex methods with particle representations of scalar fields. The focus of this paper is in describing some recent work in which the VorCat implementation of the three-dimensional vortex method [2] is applied to the grid-free analysis of two-phase particulate flows.

In view of its importance in numerous technological applications, the spatially developing planar mixing layer is used as a test bed to explore the capabilities of the grid-free technology. Numerous experimental studies (e.g., [11, 12, 14]) have been devoted to describing the vortical structures of the mixing layer including spanwise rollers, their growth and merger, the formation of braid regions and their role in creating streamwise vortex pairs that stretch and interact with the rest of the vortex system. Vortices in the mixing layer can have a significant affect on particle dispersion [8, 13], and may themselves be modified when the particle loadings are large enough.

A considerable amount of numerical work has

*VorCat is protected under U.S. Patent No. 6512999
†Professor and CTO of VorCat,Inc.
‡Senior Research Scientist, AIAA Member
§CEO, AIAA Associate Fellow

also contributed to understanding two-phase particle flow in mixing layers. Until recently (e.g. [6]) these have tended not to consider the spatially growing mixing layers that are considered in experimental studies, but rather idealizations that are more amenable to numerical treatment. In particular, 2D spatially and temporally growing mixing layers have been extensively computed [3, 9, 17, 22, 23, 24] as has temporally developing 3D mixing layer [1, 10, 15, 16, 19]. The former lack streamwise vortices, while the latter cannot fully model features associated with the spatial development, such as preferential dispersion to the slow side [9].

In the case of vortex methods, simulations have tended to be limited to the spatially growing 2D case [3, 17, 22, 23], or the transient 3D flow [1, 10] due to the impracticality of tracking enough elements to give a credible representation of the spatially developing 3D mixing layer. Recent work on these flows have been mainly done using grid-based methods. For example, Druzhinin and Elghobashi [6] apply such a scheme to modeling a relatively low Reynolds number mixing layer in which a two-fluid model is used to account for scalar dispersion including two-way coupling.

The introduction of such schemes as the Fast Multipole Method (FMM) [7] as a means of reducing the cost of velocity evaluations in vortex methods has greatly expanded their potential in the modeling of complex turbulent flows. Thus, instead of elements counted in the thousands, resolution in the millions becomes practical. In the case of the mixing layer, it is then possible to make credible simulations of the three-dimensional spatially growing turbulent mixing layer including solid particles both with and without two-way coupling between phases.

This paper presents a selection of results from a numerical simulation of the spatially developing mixing layer using the VorCat code − a commercial implementation of the vortex method specifically designed for the treatment of large scale, complex, turbulent engineering flows. The simulations reproduce many aspects of the vortex structure of mixing layers as seen in physical experiments and suggested by previous calculations of the 3D temporal case. The representation of the flow in terms of vortex elements also contributes to revealing new features of the spatially developing vortex field. The computations give new insights into the dispersion of solid particles including the effect of Stokes number and two-way coupling.

The next section describes some aspects of the numerical method, followed by discussions of how the mixing layer is modeled, the technique for modeling particle motions, two-way coupling and results for the mixing layer flow including particle dispersion.

Numerical Method

In the VorCat code the primary computational elements are vortex tubes. Accompanying these are several thin layers of fixed triangular vortex sheets adjacent to solid boundaries. The sheets are designed to capture severe vorticity gradients in the near-wall region that control the generation of vorticity in the flow field. In the present work there are no solid boundaries within the computational domain, so this aspect of the methodology is not employed.

An incentive for the use of vortex tubes, as against, for example, blob-like elements [18], is their stability in the face of vortex stretching. Thus according to Kelvin's theorem, the circulation of tubes is constant in high Reynolds number flow so the possibility of unbounded circulation, which can often occur in blob methods, is avoided.

Vortex tubes in the computation are straight-line segments whose ends are convected with the local fluid velocity thus leading to stretching and reorientation of the vorticity. Tubes that lengthen beyond a threshold are subdivided, so that the computational elements form filaments made up of chains of straight vortex elements. The allowable lengths of the tube segments establishes the finest scales that can be resolved in the flow. In this way the methodology may be thought of as a grid-free large eddy simulation (LES) technique. Sub-grid motions that are prevented from occurring entail (presumably) stretching and folding of vortex tubes as they take energy to small dissipation scales. Chorin's [4] hairpin removal and reconnection algorithms, in which folded hairpin vortices are removed, model the loss of local energy, and act as a de facto sub-grid stress model.

Summing over the individual contributions of N vortex tubes gives the velocity field $\mathbf{U}$ at a point $\mathbf{x}$ and time t as

$$\mathbf{U}(\mathbf{x},t) = -\frac{1}{4\pi}\sum_{i=1}^{N}\frac{\mathbf{r}_i \times \mathbf{s}_i}{\mid \mathbf{r}_i \mid^3}\Gamma_i \; \phi(r_i/\sigma),$$

where $\mathbf{r}_i = \mathbf{x} - \mathbf{x}_i$, $r_i = \mid \mathbf{r}_i \mid$, $\mathbf{x}_i = (\mathbf{x}_i^1 + \mathbf{x}_i^2)/2$ is the midpoint of the tube with end points $\mathbf{x}_i^1$ and $\mathbf{x}_i^2$ and $\mathbf{s}_i \equiv \mathbf{x}_i^2 - \mathbf{x}_i^1$ is an axial vector along the ith tube. In keeping with the practice of desingularizing the

Biot-Savart law [18] the smoothing function

$$\phi(r_i/\sigma) = 1 - \left(1 - \frac{3}{2}(r_i/\sigma)^3\right) e^{-(r_i/\sigma)^3}$$

appears in the velocity formula, where σ is a smoothing parameter. The effect of ϕ is confined to the region $r_i < 2.34\ \sigma$ since ϕ is unity beyond this point.

To advance the solution in time it is necessary to evaluate the velocity field over the set of end points of the tubes. This is done efficiently using a parallel implementation of the Fast Multipole Method [7]. In this scheme the tube elements are sorted using an oct-tree whose leaf nodes ideally contain approximately 100 elements. Adjacent boxes contribute to each other via the exact formula while boxes that are more distant are linked via the multipole approximation. Because of the need for smoothing, σ controls the smallest allowable box in the oct-tree, so some boxes may have more than an optimal number of elements. To maintain the speed of the overall calculation, a "middleman" scheme is adopted for the local calculations. In this, velocities are evaluated at the corner nodes of the local boxes and 3D linear interpolation used to get the local velocities. Since the latter are smooth this procedure is very accurate.

Particles

Scalar mixing problems involving massless particles are readily solved with the use of tracers that convect with the fluid and take a random walk to simulate molecular diffusion. More challenging is predicting the behavior of massed particles whose motion obeys a governing dynamical equation depending on particle size and shape, and local flow properties. If the particle loading is sufficiently small the velocity of the carrier fluid will not be affected by the presence of particles. More generally, however, it is possible to have two-way coupling between the fluid and particulate phases, where the presence of solid particles creates an apparent stress affecting the motion of the fluid phase. This is likely to be significant not only when flows with large densities of contaminants are present, but even in nominally dilute flows where particles are able to collect in large concentrations due to the organizing effect of flow structures [20].

Following the approach commonly used in other studies [3] the present effort is concerned with the dispersion of small solid spherical particles in the mixing layer under conditions in which collisions can be neglected. It is assumed that the motion of the ith particle is only affected by its drag force $\mathbf{F}_i$ so the governing dynamical equation (after scaling) is

$$\frac{d^2\mathbf{X}_i}{dt^2} = \mathbf{F}_i = \frac{1}{S_t}(1 + R_e^{2/3}/6)(\mathbf{U}(\mathbf{X}_i, t) - \mathbf{V}_i)$$

where S_t is the Stokes number, the Reynolds number $R_e = \mid \mathbf{U}(\mathbf{X}_i, t) - \mathbf{V}_i \mid d_p/\nu$, d_p is the diameter of the particles and $\mathbf{V}_i = d\mathbf{X}_i/dt$ is the velocity of the ith particle.

In the case of one-way coupling between phases the local force felt on the fluid from the presence of particles, namely $-\mathbf{F}_i$, is insufficient to cause significant change in the local velocity field. For two-way coupling the sum total of the particle forces in a given volume, say $\mathbf{F}$, becomes large enough to have a noticeable affect. In the context of the vorticity equation, the presence of particles is felt as the source term $-\nabla \times \mathbf{F}$. In keeping with the idea that the particles computed in the simulation are representative of many other particles whose motion is not explicitly computed, and the fact that the velocity field is a LES, then the affect of particles on the vorticity should be considered in a local average sense. Thus, it is assumed that the effect of particles on the flow is by generating vorticity given by evaluating $-\nabla \times \mathbf{F}$ on a collection of nearby particles. In the code, an oct-tree is grown based on the positions of particles, typically so that 4 particles are in a box. Forces at the box corners are assessed by volume weighting the contributions from particles in adjacent boxes. Then, the average contribution to vorticity generation is determined by numerically evaluating the last integral in

$$\nabla \times \mathbf{F} \approx \frac{1}{V}\int_V (\nabla \times \mathbf{F}) dV = \frac{1}{V}\int_A (\mathbf{n} \times \mathbf{F}) dA$$

which is derived using a standard vector identity. This procedure is a 3D analogue of the 2D approach taken in [23]. $\nabla \times \mathbf{F}$ can affect the flow either by changing the vorticity of pre-existing tubes or by adding new vortices to the calculation. Here the latter route is followed in the interest of simplicity.

Mixing Layer

The flow to be computed here is a planar mixing layer with velocity $U_t = 1$ in the top layer (after scaling) and velocity $U_b = 4/13$ in the bottom layer. The streamwise extent of the computational domain is the interval $0 \le x \le 3$ with vortex tubes being placed into the flow at each time step with strength $\Gamma = (1 - U_b^2)dt/2$ where dt is the time step.

The spanwise extent of the computational region is $-0.5 \leq z \leq 0.5$. This distance is subdivided into 10 equal segments for the purpose of putting new vortex tubes into the flow. Some calculations were done with 20 vortices across the span, thus effectively reducing the scale, but this did not substantially change the results. Periodicity is imposed in the spanwise direction. To enforce this condition in the context of the Biot-Savart law it is necessary to include the contributions of vortices in a number of image regions to either side of the main test section. In this study six images to each side are employed so that the velocity in the main section is determined from vortices lying in $-6.5 \leq z \leq 6.5$. The computation is made manageable using the translation properties of the FMM solver.

Accompanying the velocity field produced by vortices is a potential flow used to enforce the boundary conditions. In the present case this consists of forcing the total velocity to asymptote to U_t above the mixing layer and U_b below it. For this purpose semi-infinite vortex sheets are placed in the regions to either side of the test section, (i.e. $-\infty < x \leq 0$ and $3 \leq x \leq \infty$ with strengths/unit distance $U_t - U_b$). Calculations are initiated with $N = 36,700$ vortex tubes lying across the gap between sheets. Each of these tubes has strength $(U_t - U_b)\Delta x$ where $\Delta x = 3/N$. At each time step, a new vortex tube is introduced at $x = 0$. Those tubes that convect beyond $x = 3.1$ are removed from the flow. In a typical calculation the number of tubes increases to an equilibrium value after a period of rapid growth during transition to turbulence. For the results shown here approximately 370,000 vortex tubes are in the main test section so the total number of tubes taking into account the images is approximately 4.81 million.

Results

Structure of the Mixing Layer

The spanwise vortex tubes covering the computational region at startup evolve like a temporally growing mixing layer as they convect out of the domain. They go through a Kelvin-Helmholtz instability including vortex roll-up and pairing, followed by generation of streamwise vortices. Filling in behind the initial vortices, one spanwise vortex at a time, are vortices that over time constitute the spatially growing mixing layer. Particle seeding is done from the inlet plane beginning at time 7.5 which is well after the transient mixing layer has swept out of the flow domain.

The vortical makeup of mixing layers is strongly affected by perturbations in the incoming flow. In this way the spanwise rollers can be made to merge in various patterns and the spacing of streamwise vortex pairs appearing in the braid region can be controlled, or delayed, among other possibilities [11]. In the present calculations large flow perturbations are present due to the relative coarseness of the vortex tubes representation. This makes the numerical mixing layer experience what is tantamount to a broadband excitation lacking cyclical regularity. On the other hand, examination of the developing mixing layer over an extended time period (through $t = 12$) reveals that even though the vortex patterns change in detail, they nonetheless share common dynamical behaviors, for example, in the way in which vortices develop, become perturbed, merge and ultimately breakdown into turbulence.

Some insights into mixing layer dynamics are given in Figs. 1 - 3 containing renderings of the vortex elements appearing in the calculations. Figure 1 shows a side view of the vortex elements at a series of increasing times, while in Figs. 2 and 3 the side views at times $t = 3.65$ and 10.45 are matched with plan views. The green and red in the plan views refer to plus and minus streamwise circulation, respectively, and is determined (somewhat imprecisely) according to whether or not the end of a particular filament is upstream of downstream of its beginning. Examination of the plan views over time does indicate that the rib vortices in the braid region between rollers usually consist of counter-rotating streamwise vortex pairs. This is particularly evident in Fig. 3 where two significant rib vortices are visible in the braid region that are made up of green and red vortices lying side by side. It is also evident from Figs. 2 and 3 that some caution is needed in judging the side views in Fig. 1 since there is generally more coherency to the vortical motions than may be evident in a sideways integrated view.

The rightmost two vortices in the first image in Fig. 1 are actually part of the original transient growing mixing layer. These vortices have paired several times to get to their current size. From one image to the next in Fig. 1 the vortex system moves to the right by a little over 1/3 of the domain. A particularly clear view of this movement is visible in the third and fourth pictures where the distinct vortex to the left of the braid region in the middle at time $t = 5.35$ becomes the large structure just before the break in the mixing layer at the right at time $t = 7.05$. Figure 1 shows that there is an ever

changing pattern of vortex roll-up and merger. In particular, the x location where the new roller vortices appear varies in time. Animations show that there are periods of relative calm in the incoming vortex sheet followed by its rapid breakdown into roller vortices. Undoubtedly the apparent randomness of the vortex patterns is partly driven by upstream feed back from the instantaneous vortex field. Figure 1 also gives some idea of how the mixing layer bends toward the slower moving stream [6]. The exit direction of the inlet vortex plane shows some slight movements toward the slow moving fluid and with it vortices tend to be somewhat biased toward this side. The excursions toward the slow speed side are temporary as may be seen in the last image where the incoming mixing layer is once again level.

One source of perturbation at the inlet is created by the fixed length of the straight segments composing the incoming spanwise vortices. This controls the wavelength at which the incoming filaments can bend. This is visible in the planar views in Figs. 2 and 3, where the initially spanwise vortices are seen to kink forward at every other junction. As the vortices later agglomerate to form spanwise rollers, the spanwise undulations are heightened, and in fact, at the downstream pointing corners of the buckled vortices streamwise vorticity in the form of counter-rotating pairs are drawn out into the braid region between rollers. As this process develops, the bending of rollers becomes more pronounced. The appearance of well defined rib vortices is somewhat haphazard. As expected, the scale and spacing of streamwise vortices grows with the size of the rollers.

A particularly interesting aspect of the processes in these figures is that merging roller vortices tend to be highly kinked yet in phase alignment with each other. During merger both spanwise and streamwise vorticity appear to join into a coherent larger scale vortex. Merger of more than two vortices at once also seems to occur, yet with similar alignment of kinked vortices. Even after merger the process of streamwise vortex generation continues to occur between the large scale merged vortices, as is seen in Fig. 3.

Particle dispersion with one-way coupling

Particle dispersion under one-way coupling is investigated by seeding particles into the flow at the inlet plane $x = 0$. For simplicity, the particles are assumed to initially travel with the local fluid velocity. Particles are placed in the flow from both the vertical line $x = 0, z = 0$ and from a horizontal line $x = 0, y = 0$. The former view is one shared by 2D studies of the spatially growing mixing layer and our results confirm this work in a qualitative sense, as seen in Fig. 4 showing the position of particles released over the interval $7.5 \leq t \leq 10.75$ for calculations with $S_t = 0.001, 4$ and 100. Here blue is used to mark particles beginning in the bottom layer and red the particles in the top layer. The particles show a sensitivity to Stokes number, with maximum dispersion in the range near $S_t = 4$ due to centrifugal forces flinging particles to the outer edge of vortices. For small S_t the particles behave like fluid particles and tend to fill out the vortex cores, while at high Stokes number the particles are able to show resistance to the rollers and end up displacing a much reduced amount.

It is interesting to observe for $S_t = 4$ that the greatest dispersion into the slow moving fluid is from initially fast moving particles. This is clearly an effect of convection by the rollers. Additional insights into particle motion are contained in Figs. $5 - 7$ showing the particle positions from an initially horizontal line of particles as viewed from end-on and top for three Stokes numbers. Here, alternating red and blue colorings is done to help reveal motion and mixing in the spanwise direction. The behavior of the particles varies dramatically with S_t and shows a series of stages that reflect underlying changes in the vortical structure of the growing mixing layer. For small values of S_t the particles are drawn together into the developing spanwise roller vortices. Spanwise features reflect the different movements of particles that are pushed up or down into the fast and slow moving streams by the streamwise vortices. As the vortices grow in scale, the particles in the rollers disperse within them leading to well mixed regions that increasingly overlap downstream. Evidently, merger of the rollers enhances the uniformity of dispersion in the streamwise direction.

For $S_t = 4$ the particles are not cleared out of the braid region between the initially growing rollers to the extent that they are for $S_t = 0.001$. There appears to be a greater influence of the streamwise vortices in organizing the particles into streaks between rollers. There is then pronounced dispersion in the vertical direction by the rollers that evidently leads to a more extensive mixing by the end. When the Stokes number is large Fig. 7 shows that the most significant effect on mixing derives from the disparate streamwise velocities of particles that are pushed slightly into the fast and slower moving streams. It should be emphasized that the identical underlying vortical field is employed for all three Stokes numbers in this simulation.

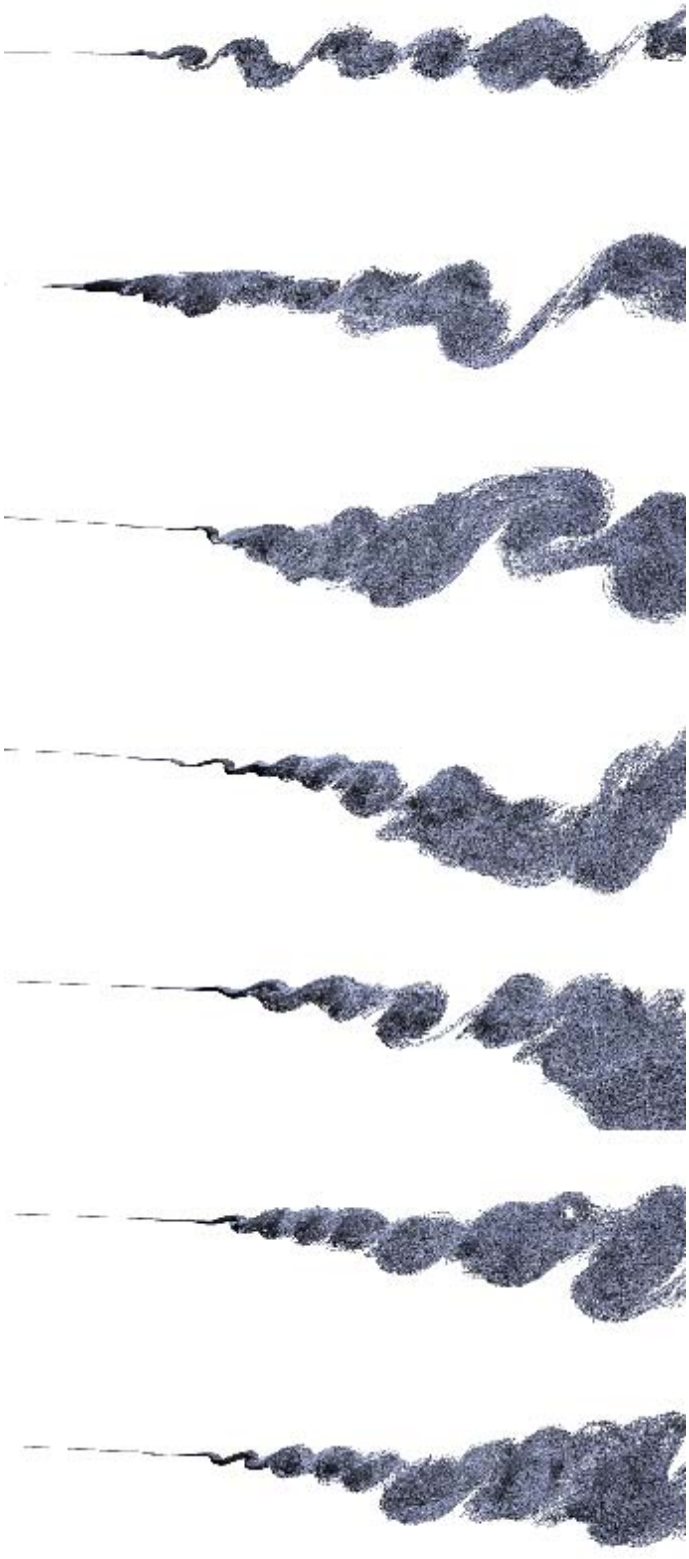

Figure 1: Side views of the mixing layer vortices at times 1.95, 3.65, 5.35, 7.05, 8.75, 10.45, 12.15

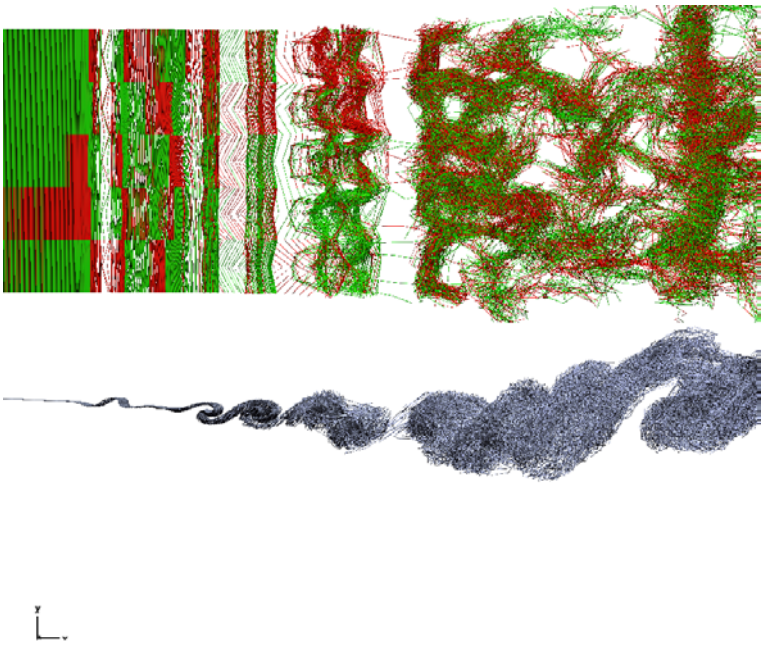

Figure 2: Top and side view of the mixing layer at time 3.65

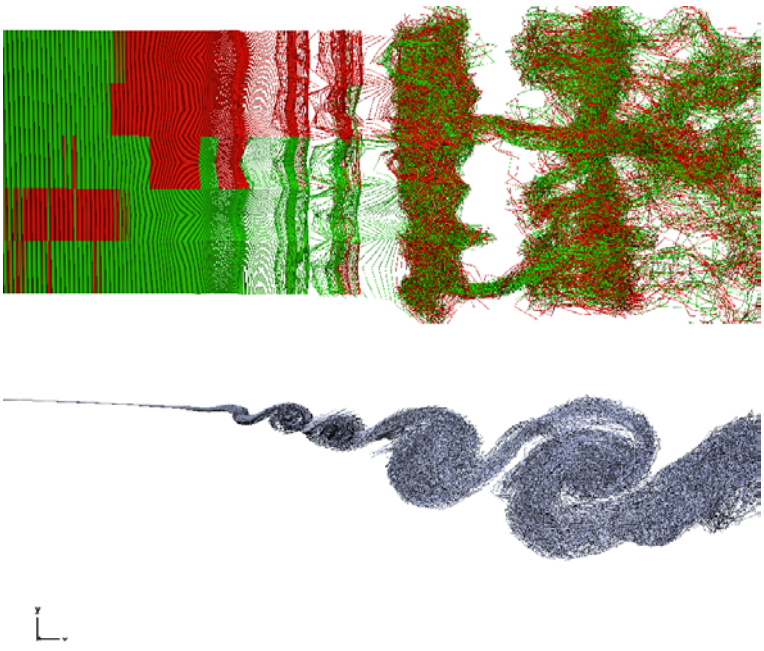

Figure 3: Top and side view of the mixing layer at time 10.45

A quantitative look at dispersion is given in Fig. 8 showing the standard deviations of the displacements of the groups of particles that were released into the flow at each time step during the time interval covered by the previous three figures. Since 101 particles are introduced at each time step, the averaging is over somewhat limited samples. Moreover, the statistics strongly reflect the particularities of the sequence of vortices and their mergers that took place during this realization of the flow. Nevertheless the figure makes clear the superior dispersion at $S_t = 4$, though interestingly enough this advantage is to some extent mitigated over time in the streamwise direction as the large vortices pair and the flow has become turbulent. For the lateral directions $S_t = 4$ has a lasting effect in enhancing dispersion, though clearly the merger events can cause the advantage to diminish, at least temporarily.

Particle dispersion with two-way coupling

The scheme for modeling two-way coupling by the introduction of new vortices has been implemented and the results will be described fully in a subsequent publication. Here space restrictions allow for including just a brief glimpse of what has been found. This is indicated in Fig. 9 showing the vortices produced via two-coupling during the very beginning stages of the calculation. The view here is of a detail of the mixing layer in the region $0 \leq x \leq 0.3$ that shows how new vortices are produced during the formation of a new roller vortex. Spanwise kinking of the roller vortex is responsible for pushing the new vortices into the fast moving stream and then form them into streamwise streaks. How this modifies the overall development of the mixing layer and dispersion will be brought out in future analysis.

Conclusions

Numerical simulation of a spatially developing 3D mixing layer including particle dispersion has been carried out using the VorCat implementation of the vortex method. Both the vortical structure of the computed mixing layer and the properties of particle dispersion with one-way coupling show much agreement with prior work. This approach was also seen to provide novel insights into the flow mechanisms that can be of considerable value in practical applications. Detailed descriptions of all aspects of this work will be provided in subsequent publications.

Acknowledgments

This material is based in part upon work supported by the National Science Foundation under grant no. 0232252. Additional support is through an ATP/NIST award to VorCat, Inc. Computer time is provided in part by NCSA.

References

[1] Ashurst, W. T. and Meiburg, E. (1988) "Three-dimensional shear layers via vortex dynamics," *J. Fluid. Mech.* **189**, 87 - 116.

[2] Bernard, P. S. and Dimas, A. A. (2001) "Vortex method modeling of complex, turbulent, engineering flows," Proc. Second International Conference on Vortex Methods, Istanbul, Turkey, September 26 - 28, pp. 41 - 54.

[3] Chein, R. and Chung J. N. (1988) "Simulation of particle dispersion in a two-dimensional mixing layer," *AIChE. J.* **34**, 946 - 954.

[4] Chorin, A. J. (1993) "Hairpin removal in vortex interactions II," *J. Comput. Phys.*, **107**, 1-9.

[5] Crowe, C. T., Troutt, T. R. and Chung, J. N. (1996) "Numerical models for two-phase turbulent flows," *Ann. Rev. Fluid. Mech.* **28**, 11.

[6] Druzhinin, O. A. and Elghobashi, S. E. (2001) "Direct numerical simulation of a three-dimensional spatially developing bubble-laden mixing layer with two-way coupling," *J. Fluid. Mech.* **429**, 23 - 61.

[7] Greengard, L., and Rokhlin, V. (1987) "A fast algorithm for particle simulations," *J. Comput. Phys.*, **73**, 325-348.

[8] Hishida, K., Ando, A. and Maeda, M. (1992) "Experiments on particle dispersion in a turbulent mixing layers," *Int. J. Multiphase Flow* **18**, 181 - 194.

[9] Hu, Z., Luo, X. and Luo, K. H. (2002) "Numerical simulation of particle dispersion in a spatially developing mixing layer," *Theor. Comput. Fluid Dyn.* **15**, 404 - 420.

[10] Knio, O. M. and Ghoniem, A. F. (1992) "The three-dimensional structure of periodic vorticity layers under non-symmetric conditions," *J. Fluid. Mech.* **243**, 353 - 392.

[11] Lasheras, J. C., Cho, J. S. and Maxworthy, T. (1986) "On the origin and evolution of streamwise vortical structures in a plane, free shear layer," *J. Fluid. Mech.* **172**, 231 - 258.

[12] Lasheras, J. C. and Choi, H. (1988) "Three-dimensional instability of a plane free shear layer: an experimental study of the formation and evolution of streamwise vortices," *J. Fluid. Mech.* **189**, 53 - 86.

[13] Lazaro, B. J. and Lasheras, J. C. (1992) "Particle dispersion in the developing free shear layer. Part 1. Unforced flow," *J. Fluid. Mech.* **235**, 143 - 178.

[14] Leboeuf, R. L and Mehta, R. D. (1996) "Vortical structure morphology in the initial region of a forced mixing layer: roll-up and pairing," *J. Fluid. Mech.* **315**, 175 - 221.

[15] Ling, W., Chung, J. N., Troutt, T. R. and Crowe, C. T. (1998) "Direct numerical simulation of a three-dimensional temporal mixing layer with particle dispersion," *J. Fluid. Mech.* **358**, 61 - 85.

[16] Luo, K., Fan. J., Jin, H. and Kefa, C. (2003) "Modulation on flow field by solid particles in gas-solid two-phase turbulent free shear flows," *Prog. Nat. Sci.* **13**, 179 - 183.

[17] Ory, E., Joia, I.A., and Perkins, R.J., "On the two-way interaction between a turbulent mixing layer and dispersed solid particles," in *Third International Conference on Multiphase Flow*, ICMF98, Lyon, France, June 8-12, 1998.

[18] Puckett, E. G. (1993) "Vortex methods: an introduction and survey of selected research topics," in *Incompressible computational fluid dynamics: trends and advances*, edited by M. D. Gunzburger and R. A. Nicolaides, Cambridge University Press, Cambridge, 335 - 407.

[19] Rogers, M. M. and Moser, R. D. (1992) "The three-dimensional evolution of a plane mixing layer: the Kelvin-Helmholtz rollup," *J. Fluid. Mech.* **243**, 183 - 226.

[20] Squires, K. D. and Eaton, J. K. (1991) "Preferential concentration of particles by turbulence," *Phys. Fluids A* **3**, 1169.

[21] Stock, D. E. (1996) "Particle dispersion in flowing gases: 1994 Freeman Scholar lecture,": *J. Fluids Eng.* **118**, 4.

[22] Tang, L, Crowe, C. T., Chung, J. N. and Troutt, T. R. (1990) "A numerical model for droplets dispersing in a developing plane shear layer including coupling effects," FED Vol. 91, ASME.

[23] Uchiyama, T. and Naruse, M. (2001) "A numerical method for gas-solid two-phase free turbulent flow using a vortex method," *Powder Tech.* **119**, 206 - 214.

[24] Wallner, E. and Meiburg, E. (2002) "Vortex pairing in two-way coupled, particle laden mixing layers," *Int. J. Multiphase Flow* **28**, 325 - 346.

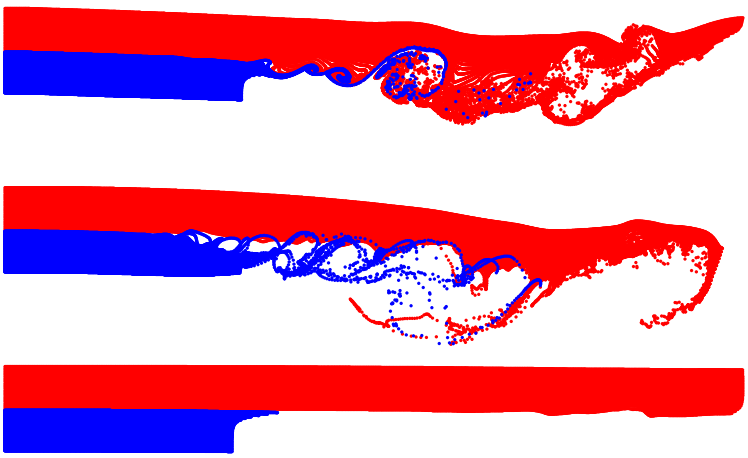

Figure 4: Side view of particles released from a vertical line during the interval $7.5 \leq x \leq 10.75$. Red and blue denote particles released in the fast and slow streams, respectively. From top to bottom figures correspond to $S_t = 0.001, 4$ and 100.

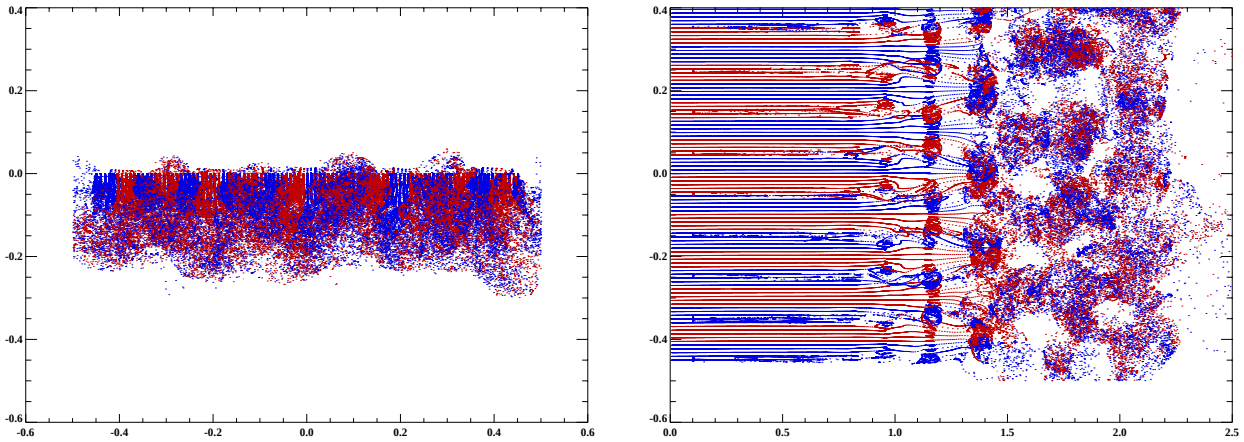

Figure 5: End-on and plan views of particles inserted on horizontal line at $y = 0$. $S_t = 0.001$.

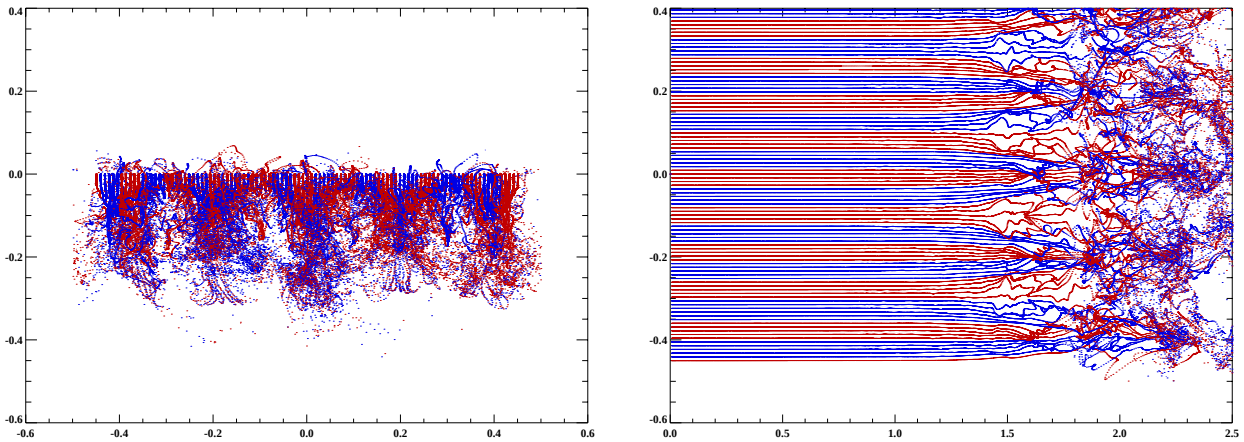

Figure 6: End-on and plan views of particles inserted on horizontal line at $y = 0$. $S_t = 4$.

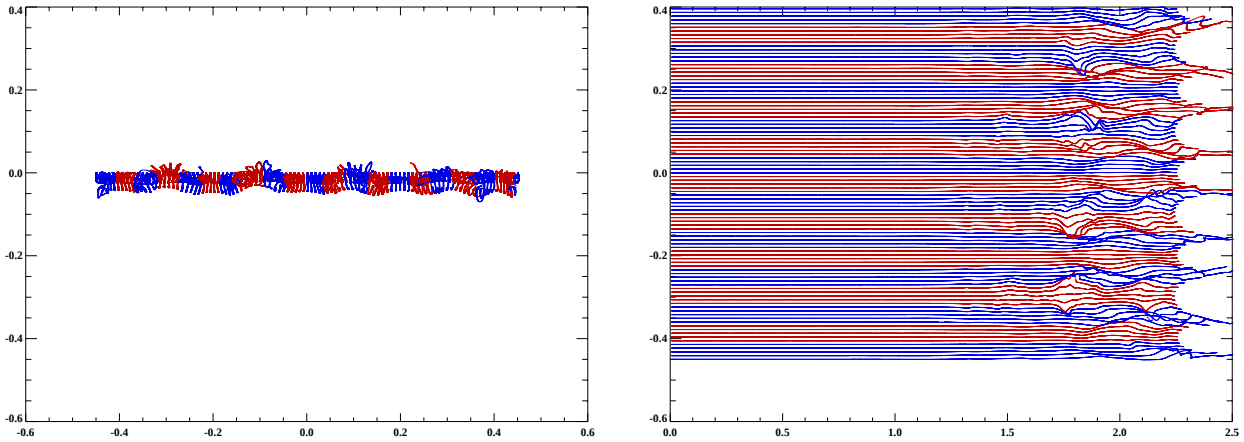

Figure 7: End-on and plan views of particles inserted on horizontal line at $y = 0$. $S_t = 100$.

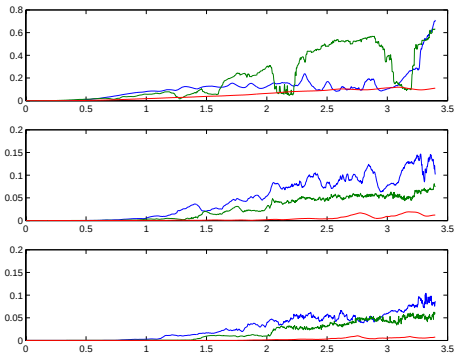

Figure 8: Standard deviation of particle dispersions. Top to bottom is x, y and z directions. $S_t = 0.001$, green; $S_t = 4$, blue; $S_t = 100$, red.

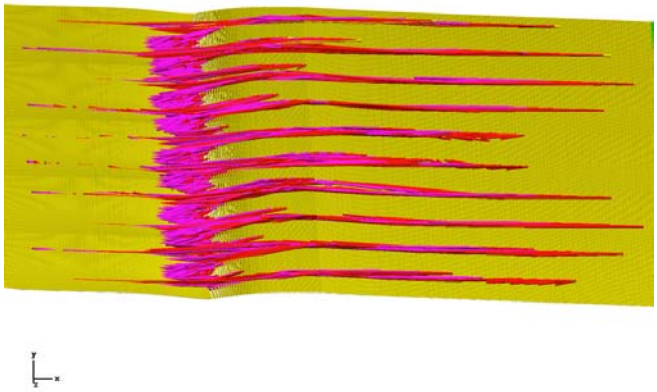

Figure 9: Detail of vortices produced by two-way coupling.